Myosin II governs intracellular pressure and traction by distinct tropomyosin-dependent mechanisms

Kimheak Sao[a], Tia M. Jones[a], Andrew D. Doyle[b], Debonil Maity[c], Galina Schevzov[d], Yun Chen[c], Peter W. Gunning[d], and Ryan J. Petrie[a,*]

[a]Department of Biology, Drexel University, Philadelphia, PA 19104; [b]National Institute of Dental and Craniofacial Research, National Institutes of Health, Bethesda, MD 20892; [c]Department of Mechanical Engineering, Johns Hopkins University, Baltimore, MD 21218; [d]School of Medical Sciences, University of New South Wales, Sydney NSW 2052, Australia

ABSTRACT **Two-dimensional (2D) substrate rigidity promotes myosin II activity to increase traction force in a process negatively regulated by tropomyosin (Tpm) 2.1. We recently discovered that actomyosin contractility can increase intracellular pressure and switch tumor cells from low-pressure lamellipodia to high-pressure lobopodial protrusions during three-dimensional (3D) migration. However, it remains unclear whether these myosin II–generated cellular forces are produced simultaneously, and by the same molecular machinery. Here we identify Tpm 1.6 as a positive regulator of intracellular pressure and confirm that Tpm 2.1 is a negative regulator of traction force. We find that Tpm 1.6 and 2.1 can control intracellular pressure and traction independently, suggesting these myosin II–dependent forces are generated by distinct mechanisms. Further, these tropomyosin-regulated mechanisms can be integrated to control complex cell behaviors on 2D and in 3D environments.**

Monitoring Editor
Carole Parent
University of Michigan

Received: Jun 12, 2018
Revised: Mar 4, 2019
Accepted: Mar 5, 2019

INTRODUCTION

Single human cells have the remarkable ability to generate forces in response to their physical environment to move efficiently. Classically, cells can sense and respond to the relative rigidity of a two-dimensional (2D) surface by increasing their actomyosin contractility (Pelham and Wang, 1997; Engler *et al.*, 2006; Prager-Khoutorsky *et al.*, 2011). Actomyosin contractility can increase tension on focal adhesion complexes to strengthen the traction applied to the extracellular environment. This traction can control adhesion size (Chrzanowska-Wodnicka and Burridge, 1996), cell velocity (Even-Ram *et al.*, 2007), and gene expression (Dupont *et al.*, 2011). Cells moving through three-dimensional (3D) extracellular matrices (ECMs) can also respond to physical and chemical signals to generate significant traction forces to align and stiffen adjacent matrix fibers and increase cell motility (Provenzano *et al.*, 2008; Calvo *et al.*, 2013; Riching *et al.*, 2014; Erdogan *et al.*, 2017).

Cells in 3D environments can also respond to the degree of matrix cross-linking by increasing actomyosin contractility to pull the nucleus forward and increase intracellular pressure (Petrie *et al.*, 2014). This increase in cytoplasmic pressure controls migratory plasticity by switching cells from using low-pressure lamellipodia to high-pressure lobopodial protrusions (Petrie *et al.*, 2012, 2017). Critically, even though the regulation of intracellular pressure and traction forces are both required for efficient cell migration, it is unclear whether these two forces can be generated simultaneously, by the same molecular machinery. Determining the molecular mechanisms generating these cellular forces will be essential to understand how cells are able to move efficiently through the structurally diverse 3D environments found in the body (Friedl *et al.*, 2012).

Both traction force and intracellular pressure are governed by the RhoA-Rho kinase (ROCK)–myosin II signaling axis (Chrzanowska-Wodnicka and Burridge, 1996; Pelham and Wang, 1999; Stewart *et al.*, 2011; Petrie *et al.*, 2014; Chengappa *et al.*, 2018). Upon activation, RhoA can bind and activate Rho kinase (ROCK; Leung

This article was published online ahead of print in MBoC in Press (http://www.molbiolcell.org/cgi/doi/10.1091/mbc.E18-06-0355) on March 13, 2019.

The authors declare no competing financial interests.

*Address correspondence to: Ryan J. Petrie (rjp336@drexel.edu).

Abbreviations used: BME, β-mercaptoethanol; CDM, cell-derived matrix; EGTA, ethylene glycol-bis(β-aminoethyl ether)-*N*,*N*,*N*′,*N*′-tetraacetic acid; F-actin, filamentous actin; FBS, fetal bovine serum; HFF, human foreskin fibroblast; KD, knockdown; Lat-A, latrunculin-A; MLC2, myosin light chain 2; NMII, nonmuscle myosin II; RT, room temperature; siRNA, small interfering RNA; TIRF, total internal reflection fluorescence; Tpm, tropomyosin.

et al., 1995). Activated ROCK phosphorylates the myosin regulatory light-chain 2 (MLC2), which can then bind and enhance NMII heavy-chain activity to generate actomyosin contractility and increase tension within the cytoskeleton (Mizutani *et al.*, 2006; Vicente-Manzanares and Horwitz, 2010). Increased tension on the dorsal and ventral stress fibers connected to focal adhesions can lead to the enlargement and maturation of focal adhesion complexes (Pasapera *et al.*, 2010) to allow the cell to exert greater traction on the ECM (Plotnikov *et al.*, 2012). Contractile actomyosin fibers can also be connected to the nucleus where increased tension facilitates the translocation of the transcriptional regulators YAP/TAZ into the nucleus (Dupont *et al.*, 2011; Elosegui-Artola *et al.*, 2017).

In 3D matrices, actomyosin contractility and the nucleus are both required for efficient cell movement (Doyle *et al.*, 2015; Graham *et al.*, 2018). Contractility overcomes matrix porosity as the rate-limiting factor of cell movement by pulling the nucleus forward, generating intracellular pressure, and sustaining lobopodia-based motility (Wolf *et al.*, 2013; Petrie *et al.*, 2017). Thus, measuring traction force, the localization of YAP/TAZ, and intracellular pressure represent three distinct approaches to quantify intracellular mechanotransduction in response to the physical environment.

The mammalian actin cytoskeleton consists of several distinct actomyosin structures that could have unique force-generating functions (Tojkander *et al.*, 2011; Burnette *et al.*, 2014; Murrell *et al.*, 2015). These morphologically distinct filamentous actin (F-actin) networks, including dorsal and ventral stress fibers, transverse arcs, and dendritic networks within lamellipodia, can also be partially distinguished by their associated tropomyosin proteins. Tropomyosins (Tpm) are a large family of actin-binding proteins that form coiled-coil polymers following each side of adjacent helical actin filaments (for a recent review, see Gunning *et al.*, 2015). For example, Tpm 1.8/9 are associated with the dendritic F-actin network to enhance the conversion of lamellipodial to lamellar actin to enable the sustained Arp2/3-mediated actin polymerization necessary for lamellipodia protrusion (Brayford *et al.*, 2016). In contrast, Tpm 2.1 is localized to dorsal and ventral stress fibers in cells on 2D, where it can control the application of myosin II–generated forces to nascent and mature focal adhesions (Tojkander *et al.*, 2011; Wolfenson *et al.*, 2016).

Here, we test the hypothesis that cellular traction against the ECM and intracellular pressure are generated by distinct mechanisms by searching for the specific Tpm isoforms responsible for governing these two cellular forces. We show that Tpm 1.6/7 expression helps to generate intracellular pressure in cells on 2D and in 3D matrices. In contrast, Tpm 2.1 expression negatively regulates traction force, but has no effect on the generation of intracellular pressure. Although both force-generating machineries can govern the recruitment of YAP/TAZ to the nucleus and are required for efficient 3D migration, we conclude that the force exerted onto the intracellular and extracellular environment can be generated by distinct, Tpm-dependent mechanisms. These distinct force-generating mechanisms are distinguished by their associated Tpm isoform and can independently control cell velocity and migratory plasticity in structurally diverse 3D environments.

RESULTS

To establish whether 2D matrix stiffness can increase focal adhesion size and cytoplasmic pressure at the same time, responses both known to require myosin II activity, we plated human foreskin fibroblasts (HFFs) on relatively soft (Young's modulus, 5 ± 2 kPa) and stiff (Young's modulus, 71 ± 17 kPa) 2D surfaces and measured the average adhesion size and intracellular pressure (P_{ic}) of each cell. We used our previously established micropressure assay (Petrie and Koo, 2014; Petrie *et al.*, 2014, 2017) to directly measure intracellular hydraulic pressure by inserting a calibrated, pressure-sensitive 0.5-µm electrode through the plasma membrane into the cytoplasm (see *Materials and Methods*). We found a significant decrease in adhesion size on soft 2D surfaces (Figure 1, A and B), as expected (Pelham and Wang, 1997; Plotnikov *et al.*, 2012). In contrast to adhesion size, we determined that intracellular pressure is increased on soft compared with stiff surfaces (Figure 1C), demonstrating that intracellular pressure and adhesion size can be independently regulated.

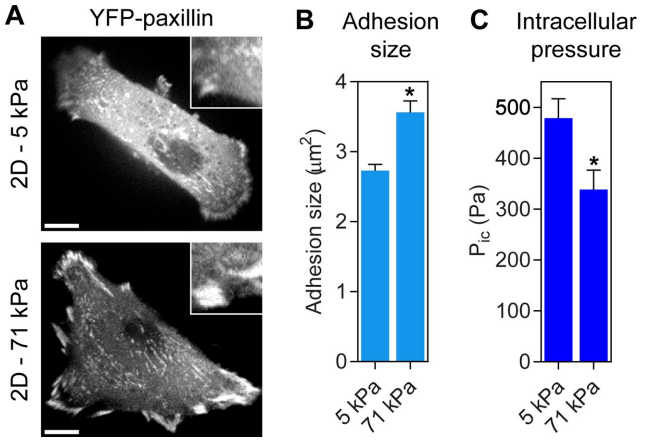

FIGURE 1: 2D matrix rigidity reciprocally regulates pressure and adhesion size. (A) Primary human dermal fibroblasts were plated on relatively soft or stiff 2D surfaces and transiently transfected with YFP-paxillin to visualize focal adhesions. Fibroblasts form larger focal adhesions on stiff (Young's modulus 71 kPa) compared with soft (5 kPa) 2D surfaces, quantified in B ($n \geq 630$, $N = 3$). Bars, 10 µm. *, $P < 0.0001$. (C) In contrast, intracellular cytoplasmic pressure (P_{ic}) significantly increases on soft 2D surfaces ($n \geq 25$, $N = 3$). *, $P < 0.02$.

Given that Tpm 2.1 negatively regulates the traction force applied to focal adhesions on 2D surfaces (Wolfenson *et al.*, 2016), we searched for a corresponding pressure-regulating tropomyosin isoform. We transiently overexpressed a panel of tropomyosins individually in HFFs on 2D glass and measured their intracellular pressure (Supplemental Figure 1). Of the tropomyosins we tested, only tGFP-Tpm1.6 expression consistently increased the intracellular pressure relative to control cells. Importantly, expression of CFP-Tpm 2.1 did not significantly affect the intracellular pressure of human fibroblasts on 2D glass compared with tGFP-Tpm 1.6 (Figure 2A), despite its established role in regulating traction force (Wolfenson *et al.*, 2016). Treatment with the myosin II inhibitor blebbistatin significantly reduced the tGFP-Tpm 1.6–mediated pressure increase (Figure 2B), indicating actomyosin contractility is required for this response. To determine whether the Tpm 1.6–dependent pressure increase corresponded with an increase in cellular traction force, Tpm transfected cells were plated on flexible microposts to measure the traction force-dependent displacement of the posts (Figure 2C). Expression of GFP-Tpm 1.6 or CFP-Tpm 2.1 both decreased traction stress (Figure 2D). Together, these data show that Tpm 1.6 and 2.1 expression can control distinct cellular mechanisms leading to independent changes in intracellular pressure and traction.

To test directly whether intracellular pressure and traction are generated by distinct mechanisms, we compared the ability of the endogenous Tpm isoforms to control pressure and traction in HFFs. Using the Tpm isoform-specific small interfering RNA (siRNA)

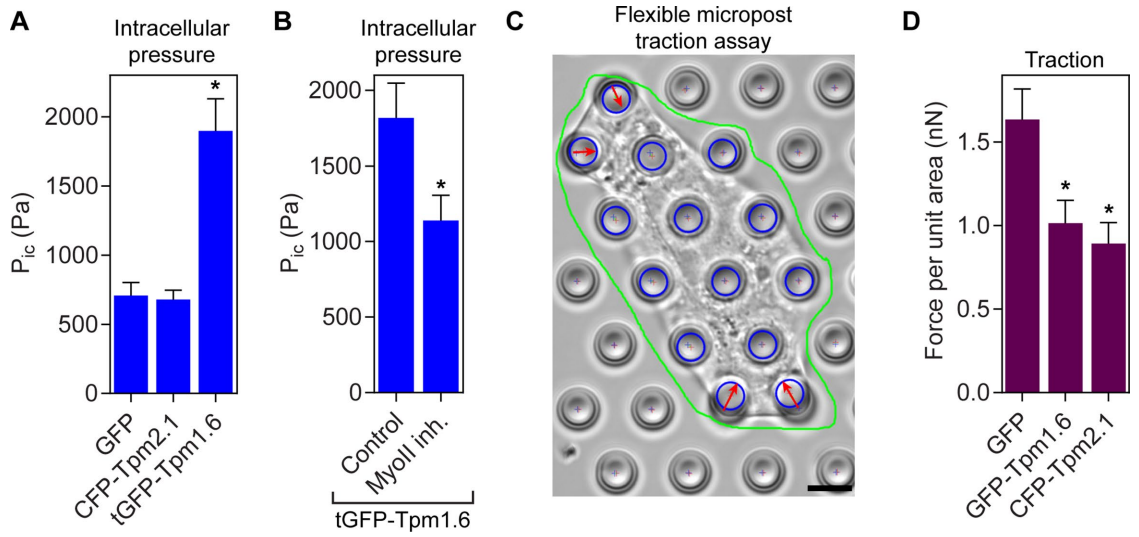

FIGURE 2: Tpm 1.6 expression in HFFs increases intracellular pressure and decreases traction stress. (A) Expression of tGFP-Tpm 1.6 in HFFs on 2D glass surfaces causes a significant elevation of intracellular pressure compared with GFP expressing control cells ($n \geq 15$, $N = 3$). *, $P < 0.0001$. (B) The increase in pressure due to tGFP-Tpm 1.6 expression is reduced by treatment with the myosin II inhibitor blebbistatin ($n = 18$, $N = 3$). *, $P < 0.03$. (C) Measuring the cell (outlined in green) -dependent displacement (red arrows) of flexible microposts of known elasticity and position allows traction stress to be calculated. (D) Expression of both GFP-Tpm 1.6 and CFP-Tpm 2.1 decrease the traction stress produced by HFFs on the flexible microposts, despite the Tpm-1.6–dependent increase in pressure measured in A ($n \geq 18$, $N = 3$). *, $P < 0.02$.

sequences previously validated (Tojkander *et al.*, 2011; Wolfenson *et al.*, 2016), we significantly reduced the expression of Tpm 1.6/7 and Tpm 2.1 in HFFs (Figure 3, A and B). There was a slight reduction in Tpm 2.1 expression following transfection of cells with the Tpm 1.6/7 siRNA. Importantly, this nonspecific knockdown of Tpm 2.1 following Tpm 1.6/7 siRNA treatment was not sufficient to affect mechanotransduction because Tpm 2.1 siRNA generated several distinct cellular phenotypes compared with Tpm 1.6/7 siRNA (Figure 3, C and D, and later in the article, Figures 6 and 7, C and D). Tpm 1.6/7 knockdown was associated with a specific reduction in MLC2 expression compared with control and Tpm 2.1 siRNA-treated cells (Figure 3, A and C), suggesting that the stability of MLC2 could be sensitive to Tpm 1.6/7 expression. In contrast, nonmuscle myosin IIA (NMIIA) heavy-chain expression was not significantly affected by loss of either Tpm 1.6/7 or 2.1.

Having established the efficacy and specificity of our Tpm knockdowns, we next measured the ability of the siRNA-treated cells to generate traction stress and intracellular pressure on a 2D surface. Tpm 2.1 knockdown significantly increased the average traction stress (2.4 ± 0.8 nN) compared with control (1.4 ± 0.6 nN) and Tpm 1.6/7 (1.3 ± 0.6 nN) siRNA-treated cells (Figure 3D), as expected (Wolfenson *et al.*, 2016). The role of Tpm 2.1 in negatively regulating traction was confirmed in a knockdown-rescue experiment performed with independent single siRNAs (Supplemental Figure 2, C, D, and G). It is not clear why the overexpression of Tpm 1.6 decreases traction stress (Figure 2D), while its knockdown has no effect (Figure 3D). Measuring the relative endogenous concentrations of Tpm 2.1 and Tpm 1.6 in these cells may help to explain this discrepancy. Critically, similarly treated cells on 2D glass exhibited no increase ($P > 0.5$, $n = 17$, where n is the total number of measurements and N corresponds to the number of independent experiments) in intracellular pressure upon loss of Tpm 2.1 or Tpm 1.6/7 (Figure 3E). Together with the Tpm overexpression studies presented in Figure 2 and Supplemental Figure 1, these data suggest that traction force can be increased without increasing intracellular pressure.

To establish a potential mechanism by which Tpm 1.6/7 and 2.1 positively and negatively regulate actomyosin contractility, respectively, we investigated the degree of Tpm association with F-actin in response to 2D substrate stiffness. On the basis of the increase in intracellular pressure (Figure 1C) and the established reduction in traction (Discher *et al.*, 2005), on softer 2D substrates, we predicted both Tpm 1.6/7 and 2.1 would be more associated with F-actin in cells on soft versus stiff surfaces. To test this prediction, we plated HFFs on soft (0.5 kPa) or stiff (64 kPa) 2D surfaces and measured the relative change to the F-actin–dependent insolubility of Tpm 1.6 and 2.1 (Meiring *et al.*, 2018). Although GAPDH was detected only in the soluble, cytoplasmic fraction isolated from cells on 2D glass, as expected (Cao *et al.*, 1999), actin, Tpm 1.6/7, and Tpm 2.1 were found in both the soluble and insoluble fractions (Figure 4, A and B). This distribution is consistent with the separation of distinct cellular pools of soluble G-actin and insoluble F-actin (Zicha *et al.*, 2003). To confirm that the insolubility of the actin and Tpms were due to the presence of polymerized actin, cells were treated with the actin depolymerizing drug latrunculin-A (Coue *et al.*, 1987). Latrunculin-A treatment significantly reduced the abundance of actin and Tpm 1.6/7 and 2.1 in the insoluble fraction, confirming that F-actin was required to maintain these proteins in the insoluble fraction.

We next compared the solubility of Tpm 1.6/7, Tpm 2.1, and the actomyosin machinery on the same relatively soft and stiff 2D surfaces. As predicted, we detected a significant reduction of Tpm 1.6/7 and 2.1 in the F-actin, insoluble fraction isolated from cells grown on 64 kPa (stiff) versus 0.5 kPa (soft) surfaces (Figure 4, C and D). In contrast, actin and NMIIA solubility was unaffected by the relative rigidity of the 2D surface (Figure 4, C and E). Interestingly, the insolubility of MLC2 was also decreased on stiffer surfaces, similar to Tpm 1.6/7 and 2.1. Together, these data suggest that the regulated association of Tpm 1.6/7 and Tpm 2.1 with actomyosin filaments in response to 2D matrix stiffness could be required for both the generation of intracellular pressure and the suppression of traction force, respectively.

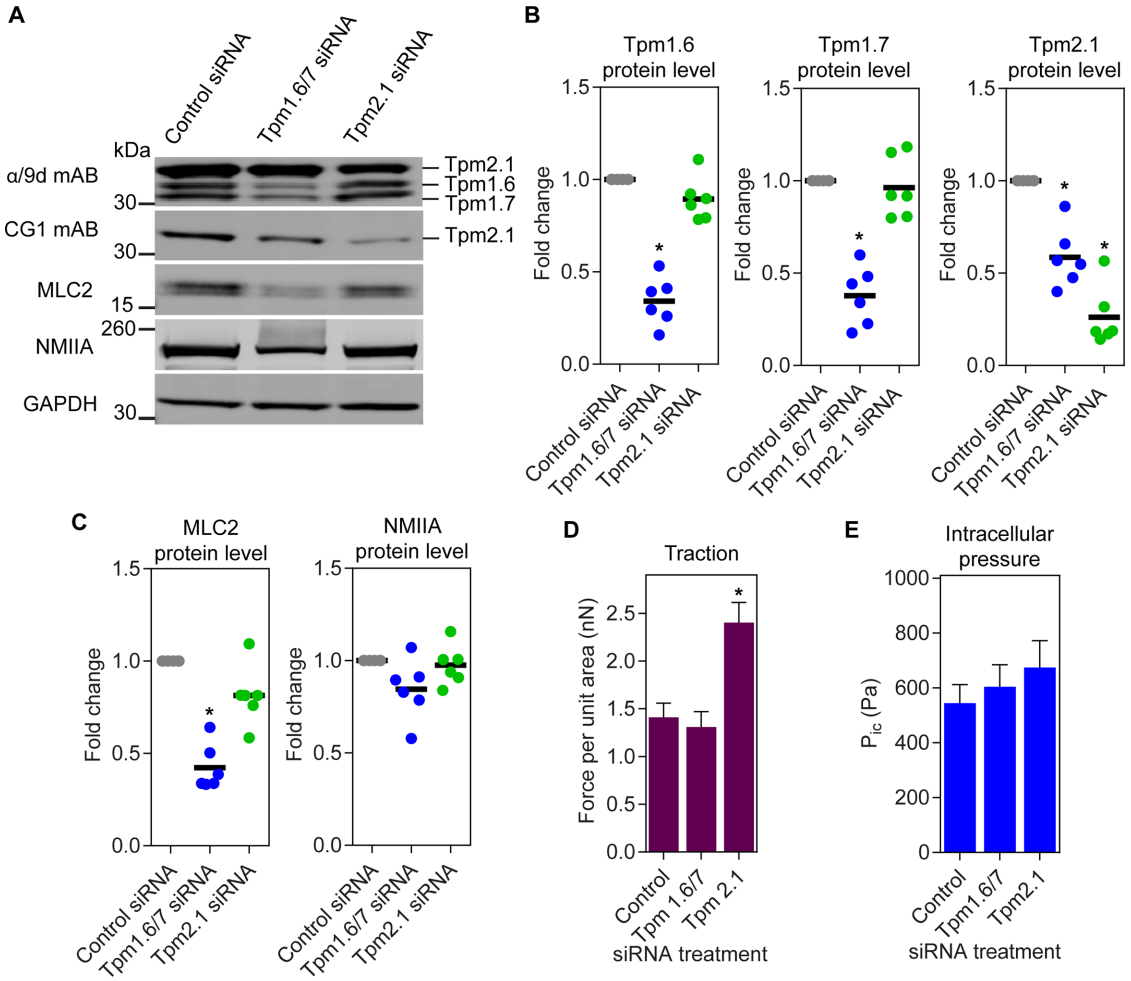

FIGURE 3: Tpm 2.1 is not required for generating intracellular pressure but is critical for governing traction stress. (A) Representative Western blots of specific tropomyosin isoforms knockdown probed with antibodies to TPM1 (α/9d mAB), Tm1 (CG1 mAB), MLC2, NMIIA, and GAPDH. (B) Quantification of specific Tpm 1.6/7- and Tpm 2.1-siRNA show reduction of specific tropomyosin isoform level with corresponding knockdown ($N = 6$). *, $P < 0.001$. (C) Quantification of MLC2 and NMIIA shows that only Tpm 1.6/7 siRNA results in reduction of MLC2 but not NMIIA ($N = 6$). *, $P < 0.001$. (D) Specific Tpm 2.1 siRNA results in an increase in traction force compared with control siRNA-treated cells ($n \geq 15$, $N = 3$). *, $P < 0.005$. (E) The treatment of HFFs plated on 2D glass with either Tpm 1.6/7 or Tpm 2.1 siRNA did not affect the generation of intracellular pressure compared with control cells ($n = 17$, $N = 3$). $P > 0.5$.

We next examined the subcellular localization of Tpm 1.6 and Tpm 2.1 in HFFs on 2D glass surfaces. We hypothesized that a difference in their localization could help to identify the population of F-actin uniquely responsible for generating either traction or intracellular pressure. HFFs moving on a 2D glass surface can possess the three dominant types of actin stress fibers (Tojkander *et al.*, 2011; Burnette *et al.*, 2014), namely, dorsal stress fibers, transverse arcs, and ventral stress fibers (Figure 5A and Supplemental Figure 3A). Despite their differential control of pressure and traction, we were unable to distinguish GFP-Tpm 1.6 and CFP-Tpm 2.1 on the basis of their subcellular localization in HFFs on 2D glass imaged using scanning confocal microscopy (Figure 5B and Supplemental Figure 3B). Both CFP-Tpm 2.1 and GFP-Tpm1.6 were found in ventral stress fibers (Tpm 2.1, 100%, $n = 30$; Tpm 1.6, 100%, $n = 30$) and dorsal stress fibers (Tpm 2.1, 68%, $n = 22$; Tpm 1.6, 100%, $n = 27$). This distribution was consistent with endogenous Tpm 1.6 and 2.1 in HFFs on 2D glass (Supplemental Figure 4) and is similar to their localization in U2OS osteosarcoma cells (Tojkander *et al.*, 2011). We then more carefully investigated their colocalization in ventral stress fibers using total internal reflection fluorescence (TIRF) microscopy. Compared to F-actin costained with two colors of phalloidin, Tpm 1.6 and 2.1 are not as colocalized, appearing to have a partially nonoverlapping distribution within large bundles of F-actin (Figure 5, C–G, and Supplemental Figure 5). Together, these results suggest that these two tropomyosin isoforms can mediate their distinct effects on intracellular pressure and adhesion size while associated, but not colocalized, within the same F-actin structure.

Given that Tpm 2.1 and Tpm 1.6/7 expression could help distinguish two myosin II–dependent force-generating mechanisms, we next determined whether these mechanisms contributed to unique cell migration phenotypes in 2D and 3D environments (Wolf *et al.*, 2003; Petrie *et al.*, 2012; Liu *et al.*, 2015). Knockdown of Tpm 1.6/7 expression significantly slowed cells moving across 2D glass surfaces, whereas the velocity of the Tpm 2.1 knockdown cells was not as consistently reduced (Figure 6, A and B). The reduced migration in response to Tpm 1.6/7 knockdown across rigid surfaces corresponded with a significant decrease in the amount of the mechanosensitive YAP/TAZ transcriptional regulators recruited into

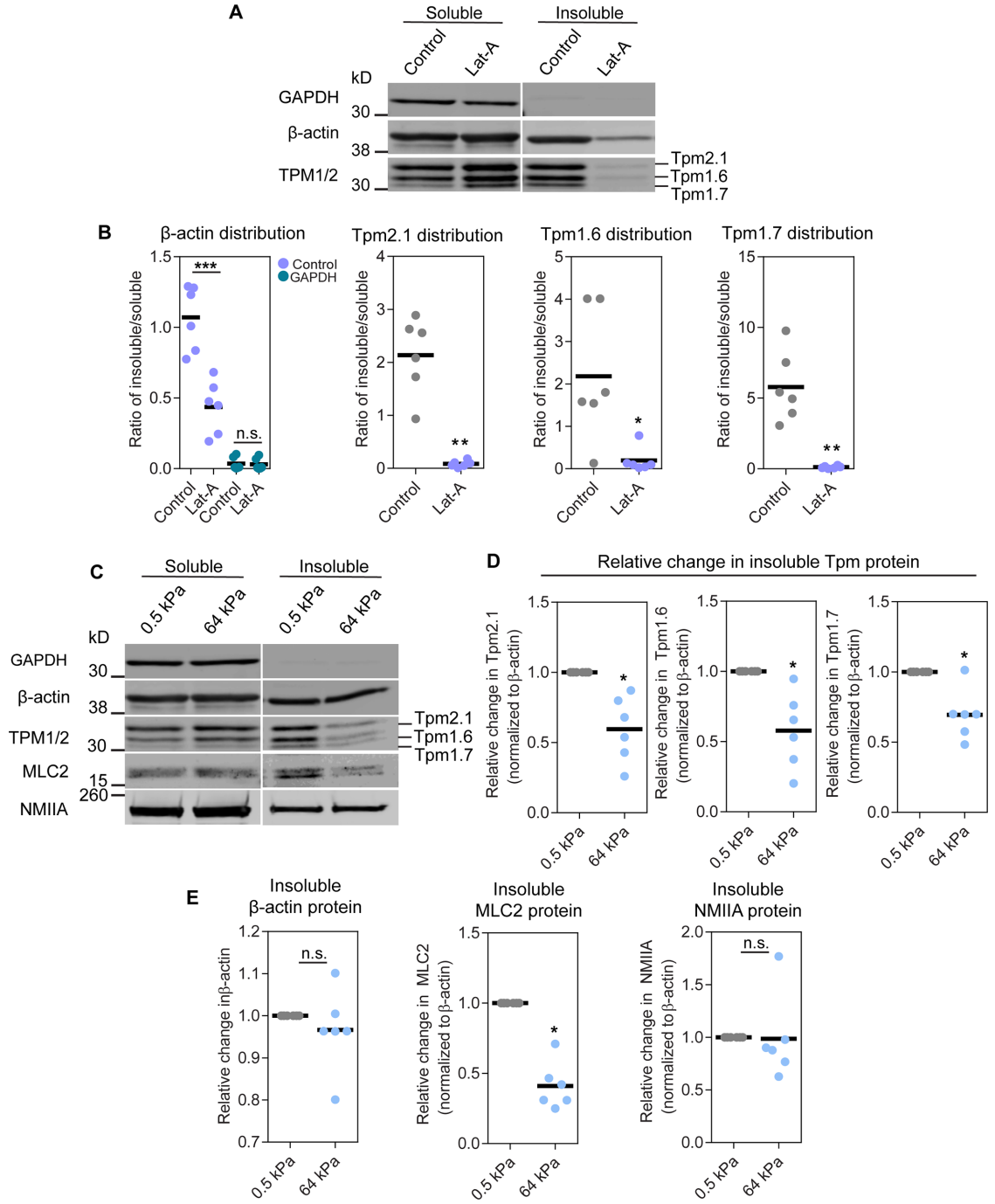

FIGURE 4: Tpm 1.6/7 and Tpm 2.1 mediate their positive and negative regulation of pressure and traction force when associated with F-actin. (A) Representative Western blots of soluble and insoluble fractions from HFFs cultured on rigid, plastic tissue culture dishes for 24 h followed with 20 μM latrunculin-A (Lat-A) treatment for 1 h before lysing. Blots were probed with antibodies to β-actin, TPM1/2 (TM311 mAB), and GAPDH. (B) Quantifications represent the ratio of the insoluble to soluble fractions of β-actin, GAPDH, and tropomyosin isoforms in control compared with Lat-A–treated cells ($N = 6$). ***, $P < 0.001$; *, $P < 0.05$; **, $P < 0.01$. (C) Representative Western blots of the soluble and insoluble fractions from HFFs cultured on 0.5 and 64 kPa 2D substrates. Blots were probed with antibodies to myosin light-chain 2 (MLC2), nonmuscle myosin heavy-chain II A (NMIIA), along with the β-actin, TPM1/2, and GAPDH antibodies described in A. (D, E) Quantifications represent relative change in the insoluble protein levels of the tropomyosin isoforms, β-actin, MLC2, and NMIIA; all are normalized to β-actin ($N = 6$). *, $P < 0.01$.

the nucleus (Figure 6, C and D). Importantly, myosin II activity is required for the nuclear localization of YAP/TAZ (Figure 6, C and D). This suggests the efficient migration of cells across rigid, 2D surfaces requires mechanotransduction downstream from Tpm 1.6. In contrast, the role of Tpm 2.1 in maintaining 2D cell velocity is less clear.

We next determined the role of Tpm 1.6/7 and Tpm 2.1 during migration in 3D environments. Because Tpm 2.1 is important for

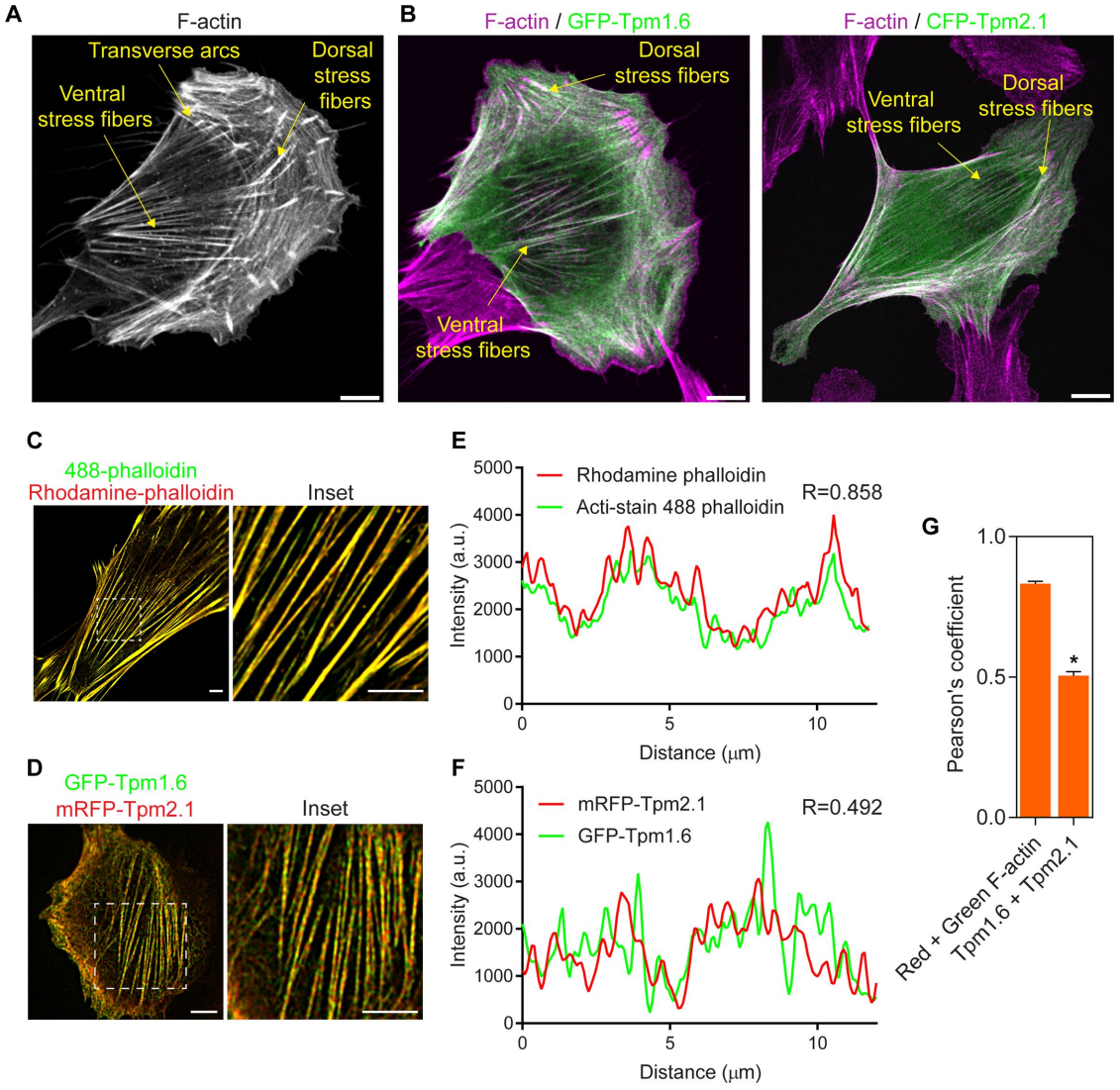

FIGURE 5: Tpm 1.6 and 2.1 are cobundled in ventral actin stress fibers. (A) The F-actin stress fiber networks within HFFs consist of ventral stress fibers, transverse arcs, and dorsal stress fibers (Tojkander *et al.*, 2011). (B) HFF transfected with GFP-Tpm1.6 shows Tpm1.6 filaments (green) bound to F-actin (magenta) and highlights their association with dorsal and ventral stress fibers. Similarly, CFP-Tpm2.1 is found predominantly in dorsal and ventral stress fibers ($n = 30$, $N = 3$). Scale bars, 10 μm. (C) Primary human fibroblasts (HFFs) were costained with rhodamine phalloidin and Acti-stain 488 phalloidin as a positive colocalization control and imaged by TIRF microscopy. (D) TIRF images of HFFs cotransfected with GFP-Tpm1.6 and mRFP-Tpm2.1. Scale bars, 5 μm. (E) Cophalloidin-labeled cell shows both red and green phalloidin intensities are more closely correlated to each other than (F) cotransfected GFP-Tpm1.6 and mRFP-Tpm2.1 as shown in representative plot profiles. (G) Pearson's correlation coefficient shows that red and green phalloidin staining on ventral stress fibers are more colocalized on the same actin bundle than GFP-Tpm1.6 and mRFP-Tpm2.1 in three independent experiments. (Control = 23 cells, 149 ventral stress fibers; co-Tpm = 25 cells, 139 ventral stress fibers). *, $P < 0.01$.

organizing actomyosin contractility during rigidity sensing on soft materials (Wolfenson *et al.*, 2016), we specifically looked for disrupted migration through soft (15 Pa, range of 11–21 Pa; Petrie *et al.*, 2012) type I collagen 3D gels (Figure 6E). In contrast to 2D glass surfaces, in the softer 3D collagen, Tpm 2.1 knockdown significantly reduced cell velocity relative to control and Tpm 1.6/7 siRNA-treated cells (Figure 6F). This reduced velocity corresponded to an increase in the recruitment of YAP/TAZ into the nucleus on soft (0.5 kPa) 2D surfaces (Figure 6, G and H). The role of Tpm 2.1 in regulating YAP/TAZ localization on soft surfaces was confirmed in a knockdown-rescue experiment performed with independent single siRNAs (Supplemental Figure 2). This increase of YAP/TAZ in the nucleus in cells on soft surfaces is consistent with the increase in traction stress measured in Tpm 2.1 knockdown cells on the flexible microposts (Figure 3D) and suggests increased contractility can slow cell movement in 3D collagen.

To determine whether endogenous Tpm 1.6 is required for high-pressure, lobopodia-based 3D migration, as suggested by its ability to increase pressure in cells on 2D glass (Figure 2A), we measured the velocity of siRNA-treated HFFs in a 3D cell-derived matrix (CDM). In contrast to soft, nonlinearly elastic 3D collagen, linearly elastic CDMs tend to be more rigid and trigger the pressure-generating,

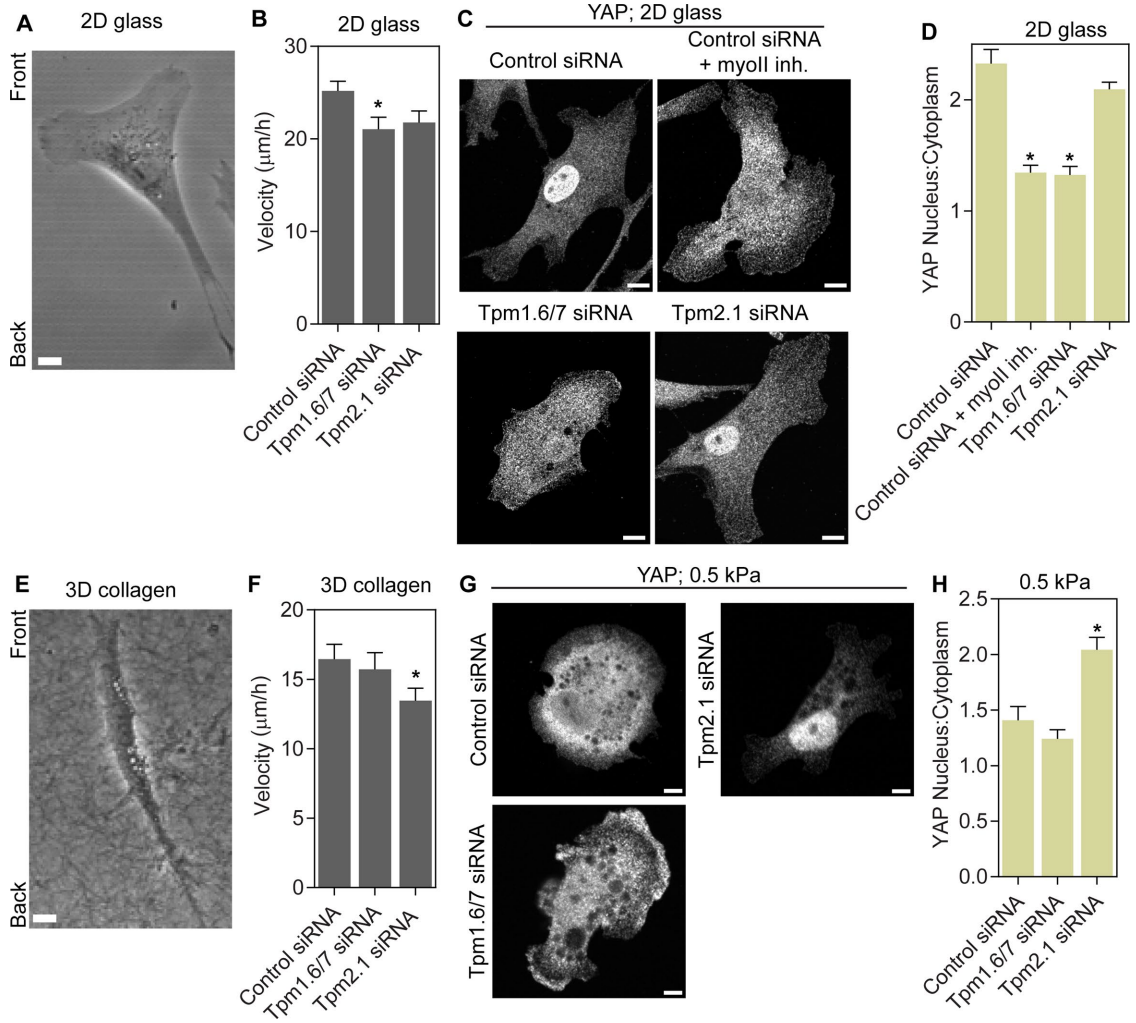

FIGURE 6: Migration in soft material requires Tpm 2.1. (A) Morphology of control primary human foreskin fibroblast (HFF) migrating on glass. Bar, 10 μm. (B) Velocity of Tpm 1.6/7 siRNA HFFs migrating on glass is significantly decreased compared with Tpm 2.1 and control siRNA cells ($n = 36$, $N = 3$). *, $P < 0.05$ vs. control cells. (C) Representative images of YAP distribution in Tpm-KD HFFs; cells were cultured on glass for 24 h before fixing and immunostaining. Bars, 10 μm. (D) Quantification of nuclear to cytoplasmic ratio of YAP in maximum projection shows a decrease in nuclear YAP in Tpm 1.6/7 siRNA or when myosin II activity is inhibited ($n = 30$, $N = 3$). *, $P < 0.001$ vs. control cells. (E) Morphology of control HFF in 1.7 mg/ml rat-tail collagen. Bar, 10 μm. (F) Decreased Tpm 2.1 expression decreases velocity in cells migrating in collagen compared with control cells ($n = 45$, $N = 3$). *, $P < 0.05$ vs. control cells. (G) Specific Tpm-KD HFFs were cultured on 0.5 kPa (soft) of stiffness for 24 h before fixing and immunostaining; shown are representative maximum projections of confocal z-stack immunofluorescence images of YAP. Bars, 10 μm. (H) Quantification of the nuclear to cytoplasmic ratio of YAP in maximum projections in cells on soft substratum shows a significant increase in nuclear YAP when Tpm 2.1 expression gets reduced compared with control ($n = 30$ total, $N = 3$). *, $P < 0.001$ vs. control cells.

nuclear piston mechanism of 3D migration in HFFs (Figure 7A; Petrie *et al.*, 2012, 2014). Tpm 1.6/7 or Tpm 2.1 siRNA-treated cells both moved significantly slower through 3D CDM compared with control cells (Figure 7B). Similarly, Tpm 1.6/7 and Tpm 2.1 were both required for targeting YAP/TAZ to the nucleus in cells in the 3D CDM (Supplemental Figure 6). In contrast, reducing Tpm 1.6/7 expression specifically switched cells from blunt, cylindrical lobopodia to lamellipodia-based migration, whereas Tpm 2.1 siRNA treatment did not affect protrusion identity (Figure 7, C and D, and Supplemental Figure 7). The role of Tpm 1.6/7 in maintaining lobopodia-based migration in 3D CDM was confirmed with an independent pool of four siRNAs (Supplemental Figure 8, A–D). These results suggest that Tpm 1.6/7 is responsible for regulating pressure in response to 2D matrix stiffness (Figure 1C) and 3D matrix elastic behavior (Petrie *et al.*, 2012), given HFFs also switch to lamellipodia in 3D when actomyosin contractility is inhibited and intracellular pressure is reduced (Petrie *et al.*, 2014).

To confirm the reduction in intracellular pressure suggested by the switch to lamellipodia-based migration (Figure 7, C and D, and Supplemental Figure 7), we treated cells in 3D CDM with the independent siRNA sequences and measured the intracellular pressure in front of the nucleus in the anterior cytoplasmic compartment (Petrie *et al.*, 2014). Knockdown of Tpm 1.6/7 reduced the anterior pressure in cells in 3D CDM (Figure 7E), demonstrating that Tpm 1.6/7 is required to generate pressure in cells migrating in 3D CDM. The role of Tpm 1.6/7 in regulating intracellular pressure in cells

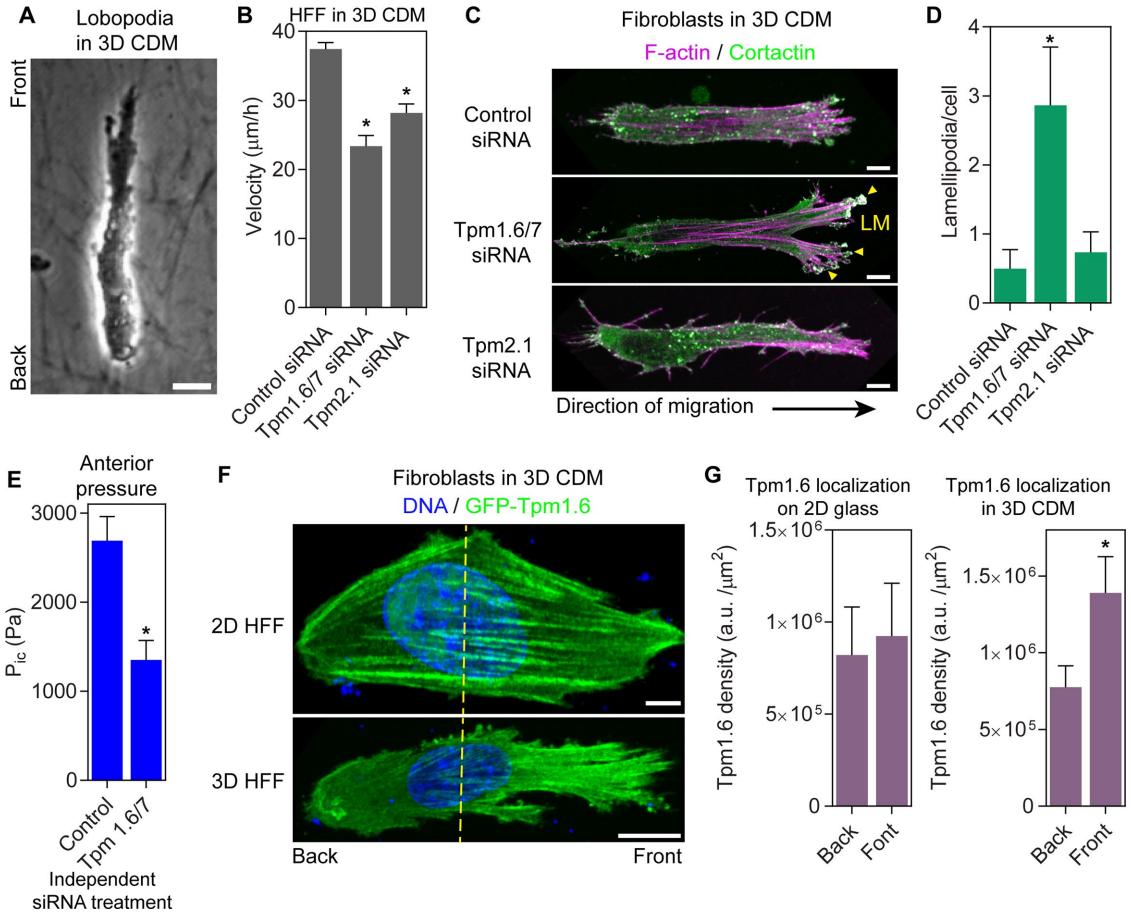

FIGURE 7: Tpm 1.6/7 is required for the nuclear piston mechanism of 3D migration and the generation of high-pressure lobopodial protrusions. (A) Representative phase image of primary human dermal fibroblast migrating in 3D CDM. Bar, 10 μm. (B) Velocity assessment of specific tropomyosin knockdown cells show Tpm1.6/7- and Tpm 2.1-siRNA–treated cells are unable to migrate efficiently in CDM compared with control cells ($n = 54$, $N = 3$). *, $P < 0.001$. (C) Tpm 1.6/7 knockdown results in an increase of lamellipodia (yellow arrowheads) indicated by an enrichment of cortactin (green) and F-actin (magenta) in leading protrusions. Bars, 10 μm. (D) Morphometric analysis of lamellipodia formed in specific tropomyosin knockdown cells ($n \geq 23$, $N = 4$). *, $P < 0.001$. (E) Knockdown of Tpm 1.6/7 significantly decreases anterior intracellular pressure in cells in 3D CDM ($n \geq 35$, $N = 3$). *, $P < 0.005$. (F) Representative images of 2D and 3D fibroblasts on and in 3D CDM transfected with GFP-Tpm 1.6, respectively. Bars, 10 μm. (G) Quantification of Tpm 1.6/7 fluorescence density in both 2D and 3D cells shows a significant increase in Tpm 1.6/7 expression in front of the nucleus in 3D lobopodial cells ($n \geq 15$, $N = 3$). *, $P < 0.05$.

migrating through 3D CDM was confirmed in a knockdown-rescue experiment performed with independent single siRNAs (Supplemental Figure 2, A and B, and Supplemental Figure 8E). Consistent with this function in generating pressure in front of the nucleus, GFP-Tpm 1.6 was concentrated in front of the cell, between the nucleus and the leading edge (Figure 7, F and G). In contrast, GFP-Tpm 1.6 was not polarized in cells moving on the 2D surface of the CDM, consistent with their previously established low-pressure, lamellipodia based on the unconfined surface of the matrix (Petrie *et al.*, 2014). Together, these results suggest that Tpm 2.1 and 1.6/7 control two distinct myosin II–dependent mechanisms responsible for unique functions in migrating cells.

DISCUSSION

On the basis of our results, we propose the association of Tpm 1.6/7 and 2.1 with F-actin is required for their positive and negative regulation of myosin II–dependent force production, respectively (Figure 8). The increased traction force resulting from dissociation of Tpm 2.1 from actomyosin fibers on stiff surfaces leads to the translocation of YAP/TAZ into the nucleus. On soft surfaces, both tropomyosin isoforms become associated with actomyosin fibers. Tpm 1.6/7–positive actomyosin fibers could help to recruit MLC2 to prebound myosin II heavy chains (Behrmann *et al.*, 2012) to increase contractility, compress the cytoplasm, and increase intracellular pressure. Taking the results together, we conclude that Tpm 1.6/7 and Tpm 2.1 can distinguish the actomyosin machineries responsible for controlling the myosin II–dependent generation of intracellular pressure and traction force, respectively.

Given that changing the expression of Tpm 1.6/7 and 2.1 is sufficient to manipulate traction force and intracellular pressure in cells moving on 2D surfaces, comparing their subcellular localization in cells could help to identify where these pathways are found. Our results suggest that at the resolution of TIRF imaging, Tpm 1.6/7 and Tpm 2.1 can be found closely associated on ventral stress fibers. Because these large actin stress fibers represent bundles of individual actin filaments (Tojkander *et al.*, 2012), we speculate that

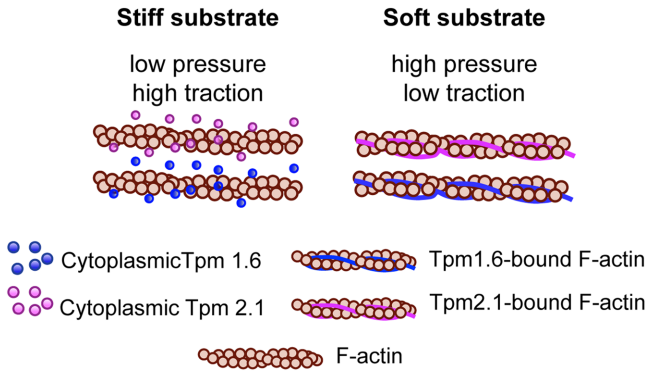

FIGURE 8: Model of the positive regulation of intracellular pressure by Tpm 1.6/7 and the negative regulation of traction force by Tpm 2.1. Mechanism 1: When fibroblasts encounter a 2D surface of increased rigidity, we propose that Tpm 2.1 (magenta) dissociates from actomyosin filaments leading to increased myosin II activity and traction force generation for efficient migration. Mechanism 2: When fibroblasts move on softer surfaces or through 3D CDM, cells have significantly higher intracellular pressure. Under these conditions, Tpm 1.6/7 (blue) is recruited to actin filaments to increase actomyosin contractility and generate intracellular pressure.

Tpm 2.1 and 1.6/7 are bound to distinct actin filaments within these bundles. In support of the concept that pressure- and traction-generating filaments may be bundled together, it has been observed that Tpm 1.6/7 and 2.1 do not overlap on the same actin filaments in vitro (Gateva *et al.*, 2017) and they can have distinct effects on F-actin elongation and stability (Janco *et al.*, 2016). Further, different Tpms can profoundly impact the functional characteristics of NMII (Barua *et al.*, 2014; Pathan-Chhatbar *et al.*, 2018). Future superresolution imaging approaches may be able to discriminate between bundled or coassembled Tpm 1.6/7 and 2.1 on actin filaments based on its previous use in determining distinct myosin II isoforms coassemble on actin filaments (Beach *et al.*, 2014) for subsequent sorting to spatially distinct actomyosin structures (Shutova *et al.*, 2017).

Although the normal regulation of traction force and intracellular pressure is required for efficient 3D cell migration (Provenzano *et al.*, 2008; Petrie *et al.*, 2014; Mekhdjian *et al.*, 2017; Owen *et al.*, 2017), our work suggests that the necessity of these pathways in migrating cells can depend on the cell's physical environment. Tpm 2.1 is specifically required for the 3D migration of HFFs through soft, randomly aligned collagen gels. Classically, myosin II activity functions to increase traction to align collagen fibers and limit the number of off-axis protrusions to enhance cell velocity (Riching *et al.*, 2014; Mekhdjian *et al.*, 2017; Owen *et al.*, 2017). We speculate that Tpm 2.1 knockdown increases cellular traction with soft materials, such as collagen and CDM (Petrie *et al.*, 2012), as evidenced by the increased recruitment of YAP/TAZ into the nucleus of cells on soft 2D surfaces, and this increased traction can act to slow 3D cell migration (Bangasser *et al.*, 2013). Crucially, Tpm 1.6/7 knockdown did not reduce cell velocity through 3D collagen gels but did slow the velocity and pressure of cells moving through 3D CDM, suggesting Tpm 1.6/7 is an integral component of the nuclear piston mechanism of high-pressure motility in CDM (Petrie *et al.*, 2014). Interestingly, Tpm 2.1 knockdown also reduced cell velocity through 3D CDM, indicating that the proper control of traction force and pressure may both be required for the nuclear piston mechanism. This is consistent with the observation that the nuclear piston mechanism also requires robust cell–matrix adhesion to generate pressure (Petrie *et al.*, 2017) and maintain velocity (Petrie *et al.*, 2012).

Together, these results suggest that intracellular pressure is not simply a by-product of the increased intracellular tension due to an elevation of actomyosin contractility. Rather, our data demonstrate that the machinery responsible for generating intracellular pressure can be controlled independently of traction force. Further, the mechanisms responsible for the generation of intracellular pressure and traction force may be activated by distinct structural features of the extracellular matrix, such as matrix rigidity and cross-linking, respectively. Ultimately, establishing the molecular details of these two tropomyosin-dependent pathways will provide an enhanced understanding of how cells respond to their physical environment to move efficiently and could lead to new therapeutic strategies to control the movement of normal and abnormal cells in the body.

MATERIALS AND METHODS

Reagents and cell culture

The following reagents were used in this study: succinimyidyl Alexa 647 (Thermo Fisher Scientific), rhodamine phalloidin (Thermo Fisher Scientific), Acti-stain 488 phalloidin (Cytoskeleton), latrunculin-A (Thermo Fisher Scientific), 4′,6-diamidine-2′-phenylindole dihydrochloride (DAPI; Thermo Fisher Scientific), and blebbistatin (EMD Millipore).

HFFs (used at passages 8–20) were maintained in phenol red–free DMEM (HyClone) containing 10% fetal bovine serum (FBS; Sigma), 4.5 g/l glucose, 100 U/ml penicillin, 100 µg/ml streptomycin, and 2 mM L-glutamine (Life Technologies) at 37°C and 10% CO_2. Collagen gels (3D; 1.7 mg/ml) and CDM were prepared as follows (Petrie *et al.*, 2012). To generate CDM, 4×10^5 HFFs were plated on gelatin-coated and glutaraldehyde-treated 35-mm glass-bottom dishes (World Precision Instruments). Cultures were maintained for 14 d, adding new media with 50 µg/ml ascorbic acid (Sigma) every other day. The matrices were denuded of cells by adding extraction buffer (20 mM NH_4OH [Sigma] and 0.5% Triton X-100 [Sigma] in phosphate buffered saline [PBS]) for 10 min at room temperature and washed with PBS. Collagen (1.7 mg/ml) was prepared by adding 10× reconstitution buffer (0.26 M $NaHCO_3$ and 0.2 M HEPES) and 10× DMEM (Invitrogen) to 10.6 mg/ml rat-tail type I collagen (BD) at a 1:1:8 ratio. The pH of the collagen mixture was adjusted to 7.5, and then diluted to 1.7 mg/ml with tissue culture medium.

siRNA sequences, cDNA constructs, and cell transfection

Knockdowns were performed using transiently transfected targeting and negative control siRNAs (Qiagen): FlexiTubeTpm 2.1 (5′-GCA CAU CGC UGA GGA UUC ATT-3′) and Tpm 1.6/7 (5′-GCU GGA GCU GGC AGA GAA ATT-3′). The specificity of the Tpm 1.6/7 siRNA was additionally confirmed using the following independent siRNA pool: (5′-CGA CGU AGC UUC UCU GAA C-3′, 5′-AGA GGU CAG UAA CUA AAU U-3′, 5′-GCA GAA GGA AGA CAG AUA U-3′, and 5′-GAA AGU CAU UGA GAG UCG A-3′). Tpm 1.6/7 ON-TARGETplus SMARTpool siRNAs, along with a nontargeting siRNA control pool, were purchased from GE Healthcare. Knockdown rescues were performed using siRNAs (Qiagen) targeting the untranslated regions of the Tpm 2.1 and 1.6/7 mRNA: Tpm 1.6/7 (5′-GGA AAG UAC AUA UCU GGG ATT-3′) and Tpm 2.1 (5′-GGU GCA CCC AGU CCG CUC ATT-3′).

HFFs (2×10^5) were transfected with a 20 nM solution of the indicated siRNA preparation using Lipofectamine 2000 (Thermo Fisher Scientific) according to the manufacturer's instructions. After 48 h,

5×10^4 siRNA-treated cells were replated on 3D CDM or glass-bottom dishes for pressure measurements or measuring adhesion size the next day, respectively. After 72 h, 1×10^5 siRNA-treated cells were plated onto flexible microposts for traction stress measurements 4 h later. YFP-paxillin was described previously (Petrie *et al.*, 2012). GFP-Tpm 1.6/7, CFP-Tpm 2.1, and GFP-Tpm 3.1 were described previously (Tojkander *et al.*, 2011). tGFP-Tpm 1.6 was purchased from Origene. mRFP-Tpm 2.1 was generated by subcloning the mammalian Tpm 2.1 into the *Xho*1-*Bam*H1 sites of mRFP-C1 (Petrie *et al.*, 2014). GFP-Tpm 1.8 and 1.9 were generated by subcloning the sequences encoding the mammalian tropomyosins into the *Bsp*EI-*Sal*I sites of pEGFP-C1 (Clontech; Brayford, 2016). All cDNAs were transfected into cells using Lipofectamine 3000 (Thermo Fisher Scientific) according to the manufacturer's instructions. All cDNAs were transfected into siRNA-treated HFFs 48 h post-siRNA treatment with the Nucleofector system (Lonza) using the P2 primary cell kit (Lonza) according to the manufacturer's instructions. The fluorescence intensity (arbitrary units) of the tropomyosin-transfected cells that were selected for live-cell measurements of intracellular pressure or traction force, was typically at the 75th percentile of all transfected cells.

Immunofluorescence labeling and imaging of fixed cells

Cells were fixed with 4% paraformaldehyde (Electron Microscopy Sciences), permeabilized with 0.25% Triton X-100, and blocked with 0.2% bovine serum albumin (BSA) in PBS. For staining with the CGβ6 antibody, cells were permeabilized on ice with chilled methanol as described (Schevzov *et al.*, 2011). All antibodies and reagents were diluted in the 0.2% BSA in PBS blocking before applying to cells. Coverslips were mounted on glass slides using Cytoseal 60 (Thermo Scientific). The following antibodies were used: mouse anti-cortactin (EMD Millipore), mouse anti-YAP (Santa Cruz), mouse anti-vinculin (Sigma), mouse anti-GAPDH (Fitzgerald), rabbit anti-MLC2 (Cell Signaling Technology), rabbit anti–β-actin (Sigma), mouse anti-TPM1 (TM311; Sigma), and rabbit anti-NMIIA (Covance). Mouse α/9d, γ/9d, CG1, and CGβ6 were described previously (Schevzov *et al.*, 2011). Cells were imaged using either a Zeiss scanning confocal microscope (510 NLO META AxioObserver Z1; Zeiss) with a Plan Apochromat 63×, 1.4 NA oil objective or an Olympus FV1000 confocal microscope with a Plan Apochromat 60×, 1.42 NA oil objective. Brightness and contrast were linearly adjusted using ImageJ 1.52b (National Institutes of Health).

For total internal reflection fluorescence (TIRF) imaging, 5×10^4 cells were seeded in 35-mm glass-bottom dishes (World Precision Instrument) with a glass thickness of 170 µm. Acti-stain 488-phalloidin and rhodamine phalloidin–labeled control cells and GFP-Tpm 1.6 and mRFP-Tpm 2.1 cotransfected cells were fixed and permeabilized as above. Cells were imaged using a DeltaVision OMX V4 inverted microscope (GE Healthcare) equipped with 60×/1.49 NA TIRF oil immersion objective lens (Olympus), 488 and 568 nm laser lines, and a sCMOS pco.edge camera (PCO). Images were acquired and aligned using softWoRx software (Version 6.1.1), before deblurring using the enhanced ratio method.

Generating flexible 2D substrates

Polydimethylsiloxane substrates of varying rigidities were prepared using a Sylgard 184 silicone elastomer kit (Dow Corning) as described (Prager-Khoutorsky *et al.*, 2011). Briefly, the silicone elastomer component was mixed with the curing agent and added to 35-mm glass-bottom dishes (Mattek). Calibrations of the substrata were performed by placing a steel ball (diameter = 0.3–0.4 mm, density = 14.95 g/cm^3; Hoover Precision, East Gramby, CT) on the substratum and measuring the resulting surface indentation (Lo *et al.*, 2000). Cross-linking of the elastomer was performed for 4 h at 70°C. Curing agent to elastomer ratios of 10:1 and 100:1 corresponded to Young's moduli 70 and 5 kPa, respectively, was used. Cross-linked elastomers were incubated with 10% FBS for 12 h at 37°C and then washed with tissue culture media. Untransfected or YFP-paxillin transfected cells (1×10^4) were plated on the flexible 2D substrates with pressure and adhesion size measurements performed the next day. YFP-paxillin was imaged using a spinning-disk confocal microscope equipped with a confocal scanning unit (CSU-X1; Yokogawa), an EM-CCD camera (C9100; Hamamatsu Photonics), a Plan Apochromat 63×, 1.4 NA oil objective (Carl Zeiss), and an environmental chamber to maintain 37°C and 10% CO_2. Focal adhesion area was measured based on thresholded YFP-paxillin images using Volocity (Perkin Elmer).

Motility assays

HFFs (1×10^4) were seeded in tissue culture media onto CDM or 1.7 mg/ml collagen gels. The following day, time-lapse movies were captured at 10% CO_2 and 37°C using a 32×, 0.4 NA Ph1 objective on a 510 NLO META AxioObserver Z1 (Zeiss). Cells were tracked every 20 min for 12 h using the Manual Tracking plug-in (F. Cordelieres, Institut Curie, Paris, France) with ImageJ 1.52b. Velocity was calculated from the tracking data using the ImageJ Chemotaxis and Migration Tool plug-in (Ibidi).

Micropressure measurements

The 900A micropressure system (World Precision Instruments) was used to make direct measurements of intracellular pressure as described previously (Petrie and Koo, 2014; Petrie *et al.*, 2017). Briefly, the micropressure system was connected to the house compressed air and vacuum lines in the Papadakis Integrated Sciences Building whose stability was monitored using a pressure manometer (World Precision Instruments). Each electrode was calibrated by immersing the tip of a 0.5-µm micropipette (World Precision Instruments) filled with 1 M KCl solution in a low-conductivity 0.1 M KCl solution within the calibration chamber (World Precision Instruments) and adjusting the resistance of the system to null or zero. The calibration chamber permits the accuracy of the 900A system to be measured by applying known pressures (established using a pressure manometer) to the side port of the chamber and monitoring the pressure detected by the system. The calibrated micropipette was then positioned using an MPC-325 micromanipulator (Sutter Instrument) within an environmental chamber (10% CO_2 and 37°C) on an AxioObserver Z1 microscope (Zeiss). To measure intracellular pressure, the microelectrode was inserted at a 45° angle into the cytoplasm, maintained in place for ≥5 s, and removed. The intracellular pressure was calculated as the average pressure reading during this time interval. For cells on 2D surfaces, the pressure was measured perinuclearly, between the nucleus and the leading edge. In 3D cells, each pressure measurement was immediately in front of the nucleus in the anterior cytoplasmic compartment (Petrie *et al.*, 2014).

Measurement of traction stress

Flexible microposts coated with an equimolar mixture of type I collagen and fibronectin were obtained from MicroDuits GmbH. The grid size, micropost diameter, and post spring constant were individually established for each of the micropost dishes used. The grid size was 12 µm, the micropost diameter ranged from 4.3 to 5.7 µm, and the spring constants ranged from 1.8 to 3.5 nN/µm between the individual dishes. Transfected fibroblasts (1×10^5) were plated per dish. The cells and posts were imaged 4 h after plating,

using a scanning confocal microscope (510 NLO META AxioObserver Z1; Zeiss) with a Plan Apochromat 63×, 1.4 NA oil objective to capture cell shape and post position. Because the diameter, position, and spring constant of the unstressed microposts were known, traction stress was calculated based on the cell-mediated changes to post position using beam theory (Tan *et al.*, 2003). Traction stress (presented as the average force per cell-contacted post) was calculated with the open source software Mechprofiler using beam theory (Goedecke *et al.*, 2015).

For the knockdown-rescue siRNA experiments we prepared silicone gels (CY 52-276 A:B = 1:1; Dow Corning) as described previously (Style *et al.*, 2013). Briefly, the silicone gels were prepared at room temperature with a Young's modulus of ~0.3 kPa and $\nu = 0.5$. The substrates were then conjugated to 0.1 µm, yellow-green fluorescent (505/515) carboxylate-modified microspheres (Thermo Fisher Scientific) at room temperature, diluted 1:25,000 in 1× PBS. The final bead solution was prepared by mixing 200 µg/ml EDC (1-ethyl-3-[3-dimethylaminopropyl] carbodiimide hydrochloride; Thermo Fisher Scientific) with the 1:25,000 bead solution diluted in 1× PBS. The 0.3 kPa substrates were coated with 2% APTS ([3-aminopropyl] triethoxysilane; Sigma-Aldrich) diluted in 1× PBS for 5 min at room temperature and then allowed to dry for 15 min at room temperature. The final bead solution was added to the surface for 2–3 h at room temperature for uniform bead density. To minimize cytotoxicity, the entire surface was the immersed in PBS for ~1 h at room temperature (Gutierrez *et al.*, 2011).

Before seeding cells, the substrates were coated with 200 µg/ml rat-tail collagen (Corning) for 1 h at 37°C. 2.5×10^4 siRNA-transfected HFFs or 1×10^5 cDNA-transfected knockdown rescue cells were plated per well and incubated for 12 h before imaging. Initial images were obtained before manually trypsinizing cells. Images were then obtained once the cells were completely detached from the surface (~10 min). Data analysis was performed using the Traction Force Microscopy plug-in for ImageJ (Tseng *et al.*, 2012).

Tropomyosin-actin association assay

HFFs (1.2×10^6) were grown on plastic 10-cm (56 cm^2) dishes as control, and HFFs (4×10^5 cells/well) were grown on a six-well plate with stiffness of 0.5 or 64 kPa (Advanced BioMatrix) for 24 h before lysing. Cells were washed briefly with warm PBS, and lysed with 500 µl of lysis and F-actin stabilization buffer (50 mM PIPES, pH 6.9, 50 mM NaCl, 5 mM $MgCl_2$, 5 mM ethylene glycol-bis(β-aminoethyl ether)-*N*,*N*,*N*′,*N*′-tetraacetic acid [EGTA], 5% glycerol, 0.1% Triton X-100, 0.1% Tween-20, 0.1% β-mercaptoethanol [BME], 0.1% Igepal CA-630, with the addition of fresh 1× protease inhibitor cocktail and 1 mM ATP) for 30 min at room temperature (RT). Cells were collected by scraping, followed by 2000 rpm centrifugation for 5 min at 37°C to pellet unbroken cells. Supernatants were then centrifuged at 50,000 rpm or $100{,}000 \times g$ for 1 h at 37°C to separate detergent-insoluble (F-actin) and soluble (G-actin) fractions, as described previously (Meiring *et al.*, 2018). Insoluble F-actin was depolymerized with an 8 M urea solution. A 4× reducing sample buffer was added to samples to make both fractions at 1× of identical volume. Soluble samples were boiled at 95°C and insoluble samples were warmed at 37°C for 5 min, and an equal volume was loaded for SDS–PAGE.

Western blotting

72 h after siRNA transfection, HFFs were lysed using RIPA buffer (1% Triton X-100, 0.5% sodium deoxycholate, 0.1% SDS, 150 mM NaCl, and 50 mM Tris, pH 8) supplemented with 1× protease inhibitors without EDTA (Roche). Cleared lysates collected were combined with an equal volume of 2× reducing sample buffer, heated to 95°C for 5 min, resolved on 4–12% Tris-glycine polyacrylamide gel (Thermo Fisher Scientific), and then transferred to nitrocellulose (0.45-µm pores). Secondary antibodies: goat anti-rabbit immunoglobulin G (IgG) Alexa 680 and goat anti-mouse IgG Alexa 680 (Thermo Fisher Scientific). Western blots were quantified by normalizing the signal intensity of the band of the protein of interest to the corresponding GAPDH signal and determining the change in expression of the siRNA-mediated protein knockdown relative to the control.

Statistical methods

Results are presented as the mean ± SEM. One-way analysis of variance with Tukey post hoc tests were used to compare three or more variables. All comparisons were performed with Prism 7 (GraphPad Software). Differences were considered statistically significant at $P < 0.05$.

ACKNOWLEDGMENTS

We thank P. Chengappa and E. Karasmanis for their suggestions on the manuscript. Research reported in this publication was supported by the National Institute of General Medical Sciences of the National Institutes of Health under Award no. R01GM126054. The content is solely the responsibility of the authors and does not necessarily represent the official views of the National Institutes of Health.

REFERENCES

Bangasser BL, Rosenfeld SS, Odde DJ (2013). Determinants of maximal force transmission in a motor-clutch model of cell traction in a compliant microenvironment. Biophys J 105, 581–592.

Barua B, Nagy A, Sellers JR, Hitchcock-DeGregori SE (2014). Regulation of nonmuscle myosin II by tropomyosin. Biochemistry 53, 4015–4024.

Beach JR, Shao L, Remmert K, Li D, Betzig E, Hammer JA 3rd (2014). Nonmuscle myosin II isoforms coassemble in living cells. Curr Biol 24, 1160–1166.

Behrmann E, Muller M, Penczek PA, Mannherz HG, Manstein DJ, Raunser S (2012). Structure of the rigor actin-tropomyosin-myosin complex. Cell 150, 327–338.

Brayford S (2016). The Regulation of Cell Motility by Tropomyosin: An Investigation into the Role of the Cytoskeletal Tropomyosins Tpm1.8/1.9 in the Regulation of Actin Dynamics at the Leading Edge of Migrating Cells. PhD Thesis. Sydney, Australia: University of New South Wales.

Brayford S, Bryce NS, Schevzov G, Haynes EM, Bear JE, Hardeman EC, Gunning PW (2016). Tropomyosin promotes lamellipodial persistence by collaborating with Arp2/3 at the leading edge. Curr Biol 26, 1312–1318.

Burnette DT, Shao L, Ott C, Pasapera AM, Fischer RS, Baird MA, Der Loughian C, Delanoe-Ayari H, Paszek MJ, Davidson MW, *et al.* (2014). A contractile and counterbalancing adhesion system controls the 3D shape of crawling cells. J Cell Biol 205, 83–96.

Calvo F, Ege N, Grande-Garcia A, Hooper S, Jenkins RP, Chaudhry SI, Harrington K, Williamson P, Moeendarbary E, Charras G, Sahai E (2013). Mechanotransduction and YAP-dependent matrix remodelling is required for the generation and maintenance of cancer-associated fibroblasts. Nat Cell Biol 15, 637–646.

Cao F, Yanagihara N, Burke JM (1999). Progressive association of a "soluble" glycolytic enzyme with the detergent-insoluble cytoskeleton during in vitro morphogenesis of MDCK epithelial cells. Cell Motil Cytoskeleton 44, 133–142.

Chengappa P, Sao K, Jones TM, Petrie RJ (2018). Intracellular pressure: a driver of cell morphology and movement. Int Rev Cell Mol Biol 337, 185–211.

Chrzanowska-Wodnicka M, Burridge K (1996). Rho-stimulated contractility drives the formation of stress fibers and focal adhesions. J Cell Biol 133, 1403–1415.

Coue M, Brenner SL, Spector I, Korn ED (1987). Inhibition of actin polymerization by latrunculin A. FEBS Lett 213, 316–318.

Discher DE, Janmey P, Wang YL (2005). Tissue cells feel and respond to the stiffness of their substrate. Science 310, 1139–1143.

Doyle AD, Carvajal N, Jin A, Matsumoto K, Yamada KM (2015). Local 3D matrix microenvironment regulates cell migration through spatiotemporal dynamics of contractility-dependent adhesions. Nat Commun 6, 8720.

Dupont S, Morsut L, Aragona M, Enzo E, Giulitti S, Cordenonsi M, Zanconato F, Le Digabel J, Forcato M, Bicciato S, *et al.* (2011). Role of YAP/TAZ in mechanotransduction. Nature 474, 179–183.
Elosegui-Artola A, Andreu I, Beedle AEM, Lezamiz A, Uroz M, Kosmalska AJ, Oria R, Kechagia JZ, Rico-Lastres P, Le Roux AL, *et al.* (2017). Force triggers YAP nuclear entry by regulating transport across nuclear pores. Cell 171, 1397–1410 e1314.
Engler AJ, Sen S, Sweeney HL, Discher DE (2006). Matrix elasticity directs stem cell lineage specification. Cell 126, 677–689.
Erdogan B, Ao M, White LM, Means AL, Brewer BM, Yang L, Washington MK, Shi C, Franco OE, Weaver AM, *et al.* (2017). Cancer-associated fibroblasts promote directional cancer cell migration by aligning fibronectin. J Cell Biol 216, 3799–3816.
Even-Ram S, Doyle AD, Conti MA, Matsumoto K, Adelstein RS, Yamada KM (2007). Myosin IIA regulates cell motility and actomyosin-microtubule crosstalk. Nat Cell Biol 9, 299–309.
Friedl P, Sahai E, Weiss S, Yamada KM (2012). New dimensions in cell migration. Nat Rev Mol Cell Biol 13, 743–747.
Gateva G, Kremneva E, Reindl T, Kotila T, Kogan K, Gressin L, Gunning PW, Manstein DJ, Michelot A, Lappalainen P (2017). Tropomyosin isoforms specify functionally distinct actin filament populations in vitro. Curr Biol 27, 705–713.
Goedecke N, Bollhalder M, Bernet R, Silvan U, Snedeker J (2015). Easy and accurate mechano-profiling on micropost arrays. J Vis Exp, doi: 10.3791/53350.
Graham DM, Andersen T, Sharek L, Uzer G, Rothenberg K, Hoffman BD, Rubin J, Balland M, Bear JE, Burridge K (2018). Enucleated cells reveal differential roles of the nucleus in cell migration, polarity, and mechanotransduction. J Cell Biol 217, 895–914.
Gunning PW, Hardeman EC, Lappalainen P, Mulvihill DP (2015). Tropomyosin—master regulator of actin filament function in the cytoskeleton. J Cell Sci 128, 2965–2974.
Gutierrez E, Tkachenko E, Besser A, Sundd P, Ley K, Danuser G, Ginsberg MH, Groisman A (2011). High refractive index silicone gels for simultaneous total internal reflection fluorescence and traction force microscopy of adherent cells. PLoS One 6, e23807.
Janco M, Bonello TT, Byun A, Coster AC, Lebhar H, Dedova I, Gunning PW, Bocking T (2016). The impact of tropomyosins on actin filament assembly is isoform specific. Bioarchitecture 6, 61–75.
Leung T, Manser E, Tan L, Lim L (1995). A novel serine/threonine kinase binding the Ras-related RhoA GTPase which translocates the kinase to peripheral membranes. J Biol Chem 270, 29051–29054.
Liu YJ, Le Berre M, Lautenschlaeger F, Maiuri P, Callan-Jones A, Heuze M, Takaki T, Voituriez R, Piel M (2015). Confinement and low adhesion induce fast amoeboid migration of slow mesenchymal cells. Cell 160, 659–672.
Lo CM, Wang HB, Dembo M, Wang YL (2000). Cell movement is guided by the rigidity of the substrate. Biophys J 79, 144–152.
Meiring JCM, Bryce NS, Wang Y, Taft MH, Manstein DJ, Liu Lau S, Stear J, Hardeman EC, Gunning PW (2018). Co-polymers of actin and tropomyosin account for a major fraction of the human actin cytoskeleton. Curr Biol 28, 2331–2337.e2335.
Mekhdjian AH, Kai F, Rubashkin MG, Prahl LS, Przybyla LM, McGregor AL, Bell ES, Barnes JM, DuFort CC, Ou G, *et al.* (2017). Integrin-mediated traction force enhances paxillin molecular associations and adhesion dynamics that increase the invasiveness of tumor cells into a three-dimensional extracellular matrix. Mol Biol Cell 28, 1467–1488.
Mizutani T, Haga H, Koyama Y, Takahashi M, Kawabata K (2006). Diphosphorylation of the myosin regulatory light chain enhances the tension acting on stress fibers in fibroblasts. J Cell Physiol 209, 726–731.
Murrell M, Oakes PW, Lenz M, Gardel ML (2015). Forcing cells into shape: the mechanics of actomyosin contractility. Nat Rev Mol Cell Biol 16, 486–498.
Owen LM, Adhikari AS, Patel M, Grimmer P, Leijnse N, Kim MC, Notbohm J, Franck C, Dunn AR (2017). A cytoskeletal clutch mediates cellular force transmission in a soft, three-dimensional extracellular matrix. Mol Biol Cell 28, 1959–1974.
Pasapera AM, Schneider IC, Rericha E, Schlaepfer DD, Waterman CM (2010). Myosin II activity regulates vinculin recruitment to focal adhesions through FAK-mediated paxillin phosphorylation. J Cell Biol 188, 877–890.
Pathan-Chhatbar S, Taft MH, Reindl T, Hundt N, Latham SL, Manstein DJ (2018). Three mammalian tropomyosin isoforms have different regulatory effects on nonmuscle myosin-2B and filamentous beta-actin in vitro. J Biol Chem 293, 863–875.
Pelham RJ Jr, Wang Y (1997). Cell locomotion and focal adhesions are regulated by substrate flexibility. Proc Natl Acad Sci USA 94, 13661–13665.
Pelham RJ Jr, Wang Y (1999). High resolution detection of mechanical forces exerted by locomoting fibroblasts on the substrate. Mol Biol Cell 10, 935–945.
Petrie RJ, Gavara N, Chadwick RS, Yamada KM (2012). Nonpolarized signaling reveals two distinct modes of 3D cell migration. J Cell Biol 197, 439–455.
Petrie RJ, Harlin HM, Korsak LI, Yamada KM (2017). Activating the nuclear piston mechanism of 3D migration in tumor cells. J Cell Biol 216, 93–100.
Petrie RJ, Koo H (2014). Direct measurement of intracellular pressure. Curr Protoc Cell Biol 63, 12.9.1-9.
Petrie RJ, Koo H, Yamada KM (2014). Generation of compartmentalized pressure by a nuclear piston governs cell motility in a 3D matrix. Science 345, 1062–1065.
Plotnikov SV, Pasapera AM, Sabass B, Waterman CM (2012). Force fluctuations within focal adhesions mediate ECM-rigidity sensing to guide directed cell migration. Cell 151, 1513–1527.
Prager-Khoutorsky M, Lichtenstein A, Krishnan R, Rajendran K, Mayo A, Kam Z, Geiger B, Bershadsky AD (2011). Fibroblast polarization is a matrix-rigidity-dependent process controlled by focal adhesion mechanosensing. Nat Cell Biol 13, 1457.
Provenzano PP, Inman DR, Eliceiri KW, Trier SM, Keely PJ (2008). Contact guidance mediated three-dimensional cell migration is regulated by Rho/ROCK-dependent matrix reorganization. Biophys J 95, 5374–5384.
Riching KM, Cox BL, Salick MR, Pehlke C, Riching AS, Ponik SM, Bass BR, Crone WC, Jiang Y, Weaver AM, *et al.* (2014). 3D collagen alignment limits protrusions to enhance breast cancer cell persistence. Biophys J 107, 2546–2558.
Schevzov G, Whittaker SP, Fath T, Lin JJ, Gunning PW (2011). Tropomyosin isoforms and reagents. Bioarchitecture 1, 135–164.
Shutova MS, Asokan SB, Talwar S, Assoian RK, Bear JE, Svitkina TM (2017). Self-sorting of nonmuscle myosins IIA and IIB polarizes the cytoskeleton and modulates cell motility. J Cell Biol 216, 2877–2889.
Stewart MP, Helenius J, Toyoda Y, Ramanathan SP, Muller DJ, Hyman AA (2011). Hydrostatic pressure and the actomyosin cortex drive mitotic cell rounding. Nature 469, 226–230.
Style RW, Hyland C, Boltyanskiy R, Wettlaufer JS, Dufresne ER (2013). Surface tension and contact with soft elastic solids. Nat Commun 4, 2728.
Tan JL, Tien J, Pirone DM, Gray DS, Bhadriraju K, Chen CS (2003). Cells lying on a bed of microneedles: an approach to isolate mechanical force. Proc Natl Acad Sci USA 100, 1484–1489.
Tojkander S, Gateva G, Lappalainen P (2012). Actin stress fibers—assembly, dynamics and biological roles. J Cell Sci 125, 1855–1864.
Tojkander S, Gateva G, Schevzov G, Hotulainen P, Naumanen P, Martin C, Gunning PW, Lappalainen P (2011). A molecular pathway for myosin II recruitment to stress fibers. Curr Biol 21, 539–550.
Tseng Q, Duchemin-Pelletier E, Deshiere A, Balland M, Guillou H, Filhol O, Thery M (2012). Spatial organization of the extracellular matrix regulates cell-cell junction positioning. Proc Natl Acad Sci USA 109, 1506–1511.
Vicente-Manzanares M, Horwitz AR (2010). Myosin light chain mono- and diphosphorylation differentially regulate adhesion and polarity in migrating cells. Biochem Biophys Res Commun 402, 537–542.
Wolf K, Mazo I, Leung H, Engelke K, von Andrian UH, Deryugina EI, Strongin AY, Brocker EB, Friedl P (2003). Compensation mechanism in tumor cell migration: mesenchymal-amoeboid transition after blocking of pericellular proteolysis. J Cell Biol 160, 267–277.
Wolf K, Te Lindert M, Krause M, Alexander S, Te Riet J, Willis AL, Hoffman RM, Figdor CG, Weiss SJ, Friedl P (2013). Physical limits of cell migration: control by ECM space and nuclear deformation and tuning by proteolysis and traction force. J Cell Biol 201, 1069–1084.
Wolfenson H, Meacci G, Liu S, Stachowiak MR, Iskratsch T, Ghassemi S, Roca-Cusachs P, O'Shaughnessy B, Hone J, Sheetz MP (2016). Tropomyosin controls sarcomere-like contractions for rigidity sensing and suppressing growth on soft matrices. Nat Cell Biol 18, 33–42.
Zicha D, Dobbie IM, Holt MR, Monypenny J, Soong DY, Gray C, Dunn GA (2003). Rapid actin transport during cell protrusion. Science 300, 142–145.